

DOI: 10.1002/adma.200501447

# Direct-Write Assembly of Three-Dimensional Photonic Crystals: Conversion of Polymer Scaffolds to Silicon Hollow-Woodpile Structures\*\*

By Gregory M. Gratson, Florencio García-Santamaría, Virginie Lousse, Mingjie Xu, Shanhui Fan, Jennifer A. Lewis,\* and Paul V. Braun\*

Impressive developments in silicon microfabrication are enabling new applications in photonics,<sup>[1–4]</sup> microelectromechanical systems (MEMS),<sup>[5]</sup> and biotechnology.<sup>[6,7]</sup> Yet conventional<sup>[8]</sup> Si microfabrication techniques require expensive masks and time-consuming procedures, including multiple planarization<sup>[9]</sup> or bonding<sup>[10]</sup> steps, to generate three-dimensional (3D) structures. In contrast, direct-write approaches,<sup>[11]</sup> such as laser scanning<sup>[12,13]</sup> and ink deposition,<sup>[14]</sup> provide rapid, flexible routes for fabricating 3D microperiodic structures. However, these approaches are currently limited to polymeric structures that lack the high refractive index contrast and mechanical integrity required for many applications. To take full

advantage of these rapid, flexible assembly techniques, one must develop a replication (or templating) scheme that enables their structural conversion within the temperature constraints imposed by both the organic and inorganic components of the system. Here, we present a novel route for creating 3D Si hollow-woodpile structures that couples direct-write assembly of concentrated polyelectrolyte inks<sup>[14,15]</sup> with a sequential silica<sup>[16]/Si<sup>[17]</sup></sup> chemical vapor deposition (CVD) process. The optical properties of the 3D microperiodic woodpiles are characterized after each fabrication step. These interconnected, hollow structures may find potential application as photonic materials,<sup>[18]</sup> low-cost MEMS,<sup>[19]</sup> microfluidic networks for heat dissipation,<sup>[20]</sup> and biological devices.<sup>[21]</sup>

Since the concept of a photonic bandgap (PBG)<sup>[22,23]</sup> was first introduced, there has been intense interest in generating 3D microperiodic structures composed of alternating high- and low-refractive-index materials.<sup>[18]</sup> Si is an ideal material for photonic crystals, because it has a high refractive index ( $n \sim 3.45$ ) and is optically transparent in the infrared. The woodpile structure,<sup>[24,25]</sup> which consists of a 3D array of orthogonally stacked rods, is particularly well suited to microfabrication<sup>[9]</sup> and direct-write assembly<sup>[13]</sup> techniques. Engineered defects that add functionality to photonic crystals can also be readily incorporated into woodpile structures. For example, waveguides containing 90° bends can be formed by simply removing two orthogonal filaments in adjacent layers.<sup>[26]</sup> In contrast, it is inherently difficult to introduce controlled defects into inverse face-centered cubic structures produced by colloidal self-assembly routes. Additional processing steps, such as two-photon polymerization,<sup>[27]</sup> are necessary to impart the desired functionality to these structures.

3D microperiodic polymer scaffolds are fabricated in a woodpile architecture via direct-write assembly of a concentrated polyelectrolyte ink in a layer-by-layer build sequence<sup>[14]</sup> (Fig. 1). 8- and 16-layer woodpile structures ranging in lateral dimensions from 250  $\mu\text{m} \times 250 \mu\text{m}$  to 500  $\mu\text{m} \times 500 \mu\text{m}$  were formed with in-plane center-to-center rod spacings ( $d$ ) of 2.8  $\mu\text{m}$  and 4.0  $\mu\text{m}$ , and a rod diameter of 1  $\mu\text{m}$ . These dimensions do not represent the limit of the direct-writing process, where the maximum lateral dimensions can exceed 1 cm  $\times$  1 cm, rod diameters can be as low as 600 nm, and rods can be close packed on a pitch that equals the rod dimension.<sup>[14,15]</sup> Our ink design utilizes concentrated polyelectrolyte complexes composed of a non-stoichiometric mixture<sup>[28]</sup> of

[\*] Prof. J. A. Lewis, Prof. P. V. Braun, Dr. G. M. Gratson, Dr. F. García-Santamaría  
Beckman Institute for Advanced Science and Technology,  
Department of Materials Science and Engineering, and  
Frederick Seitz Materials Research Laboratory  
University of Illinois at Urbana-Champaign  
Urbana, IL 61801 (USA)  
E-mail: jalewis@uiuc.edu; pbraun@uiuc.edu

Prof. J. A. Lewis, M. Xu  
Department of Chemical and Biomolecular Engineering,  
Department of Materials Science and Engineering, and  
Frederick Seitz Materials Research Laboratory  
University of Illinois at Urbana-Champaign  
Urbana, IL 61801 (USA)

Dr. V. Lousse, Prof. S. Fan  
Department of Electrical Engineering  
Stanford University  
Stanford, CA 94305-4088 (USA)

Dr. V. Lousse  
Laboratoire de Physique du Solide  
Facultés Universitaires Notre-Dame de la Paix  
B-5000 Namur (Belgium)

[\*\*] G. M. Gratson and F. García-Santamaría contributed equally to this work. This material is based in part on work supported by the U.S. Department of Energy, Division of Materials Sciences, under Award No. DEFG-02-91ER45439, through the Frederick Seitz Materials Research Laboratory at the University of Illinois at Urbana-Champaign, and the U.S. Army Research Laboratory and the U.S. Army Research Office under contract/grant number DAAD19-03-1-0227, and was carried out in part in the Center for Microanalysis of Materials, University of Illinois, which is partially supported by the U.S. Department of Energy under grant DEFG02-91-ER45439. V. L. was supported in part as Postdoctoral Fellow by the Belgian National Fund for Scientific Research (FNRS).

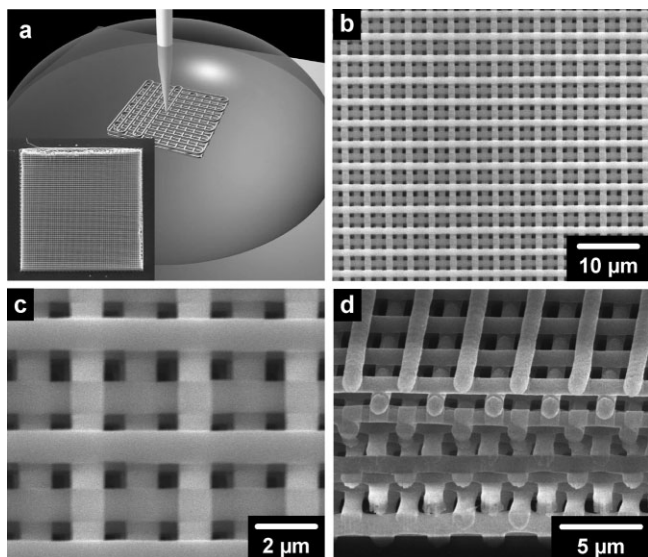


**Figure 1.** a) Schematic illustration (inset is a low-magnification scanning electron microscopy (SEM) image of a  $250\ \mu\text{m} \times 250\ \mu\text{m}$  woodpile structure) and b–d) SEM images of direct-write-assembled polymer woodpile structures: b) intermediate-magnification top view; c) high-magnification top view showing the high degree of registry between layers, where lower layers can just be seen in the upper right of each hole because the sample is slightly tilted; d) focused ion beam milled cross section showing the excellent alignment between layers. Polymer woodpile is a 16-layer structure, in-plane center-to-center rod spacings  $d = 4\ \mu\text{m}$ .

poly(acrylic acid) and poly(ethylenimine). Through careful design,<sup>[29]</sup> we produce homogeneous fluids (40 wt.-% polyelectrolyte in aqueous solution) with the requisite viscosity ( $\eta = 7.6\ \text{Pa s}$ ) needed for deposition through microcapillary nozzles.<sup>[15]</sup> Upon deposition into an alcohol-rich reservoir, the ink rapidly solidifies, yielding a cylindrical filament whose diameter is approximately equal to the nozzle size.<sup>[14,15]</sup> The deposited filaments maintain their cylindrical shape while spanning unsupported regions in the woodpile structure, yet adhere to both the substrate and underlying layers. As can be observed in Figure 2b, the bottom layer of the polymer scaffold can sometimes be compressed perpendicular to the substrate during the writing process; however, this effect lessens substantially after printing of the initial layer.

To generate a woodpile with strong photonic effects, it is necessary to enhance the refractive index contrast; for example, by infilling some of the void space with Si. However, the polymer scaffolds cannot withstand the temperature conditions necessary for Si CVD, and thus a sequential deposition process is utilized (Fig. 2d). First, an 8-layer polymer woodpile lattice ( $d = 2.8\ \mu\text{m}$ ) is coated with a  $\sim 100\ \text{nm}$  thick silica layer via a room-temperature CVD process.<sup>[12]</sup> The polymer scaffold is subse-

quently removed by heating the sample at  $475\ ^\circ\text{C}$  for 3 h in air. This results in a  $\text{SiO}_2$  hollow-woodpile that can now withstand the processing temperatures required for Si CVD (Fig. 2a). Next, the  $\text{SiO}_2$  hollow-woodpile is coated with  $\sim 100\ \text{nm}$  of Si via CVD. Si deposits on both the inside and outside of the  $\text{SiO}_2$  tubular array, generating the trilayer coating illustrated schematically in the lower left of Figure 2d. This trilayer coating is best observed in the contrast-enhanced region of the hollow cylinder cross section shown in Figure 2c. A darker ( $\text{SiO}_2$ ) band resides between two lighter (Si) bands, in which the outer band appears to be slightly thicker than the inner band. This difference in Si band thickness is expected, given that the disilane precursor has greater access to the outer cylinder surface as compared to the inner surface. Because the initial polymer template is interconnected in all three dimensions, the resulting hollow-woodpile formed after the  $\text{SiO}_2/\text{Si}$  CVD process comprises an interconnected array of cylinders that possess a total wall ( $\text{Si}/\text{SiO}_2/\text{Si}$ ) thickness of  $\sim 300\ \text{nm}$  (Figs. 2b,c).

The intensity and spectral position of the optical features from polymer woodpile structures depend on the scaffold geometry. Figure 3 presents experimental and simulated reflectance spectra of 8- and 16-layer polymer scaffolds with  $d$  values of  $2.8\ \mu\text{m}$  and  $4.0\ \mu\text{m}$ , respectively. As expected, doubling of the number of layers in the scaffold results in an increase of the intensity and sharpness of the optical features. In addition, the peak shifts to longer wavelength ( $\lambda$ ) as  $d$  increases. Both observations are in good agreement with our simulations as well as experimental results reported for other woodpile structures.<sup>[9,13]</sup> The correlation between experiment and simulation indicate the overall quality of the structures is rather good. Although the intensity of the experimentally ob-

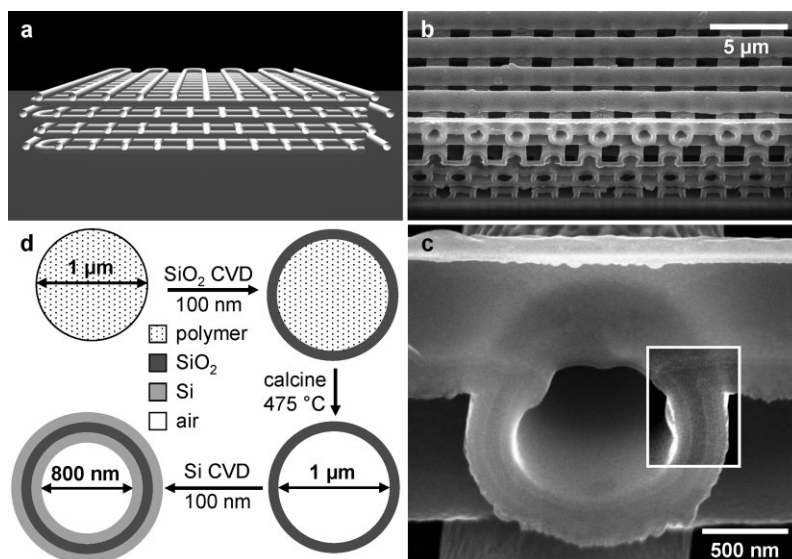


**Figure 2.** a) Schematic illustration of a hollow-woodpile structure. b) Low- and c) high-magnification SEM images of a  $\text{Si}/\text{SiO}_2/\text{Si}$  hollow-woodpile structure after focused ion beam milling (8-layer structure,  $d = 2.8\ \mu\text{m}$ ). Contrast enhanced in inset in (c) to reveal trilayer tube wall. d) Process sequence for templated assembly of such structures.

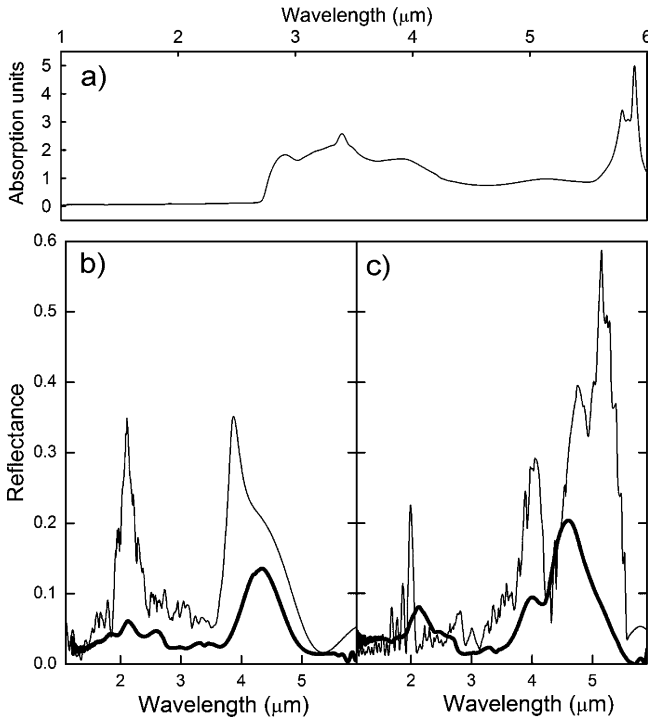


**Figure 3.** a) Absorption spectrum for a 50  $\mu\text{m}$  thick polymer film. b,c) Measured (thick line) and simulated (thin line) reflectance spectra for polymer woodpile structures: b) 8-layer structure,  $d=2.8 \mu\text{m}$ ; c) 16-layer structure,  $d=4.0 \mu\text{m}$ .

served reflectance peaks is less than the simulated values, this may be due in part to strong polymer absorption at  $\lambda > 2.7 \mu\text{m}$  that attenuates the reflectance peaks (Fig. 3a).

Following room-temperature  $\text{SiO}_2$  deposition and polymer removal, the optical properties of the  $\text{SiO}_2$  hollow-woodpile are measured and compared with simulations (Fig. 4). The agreement between the experimental and simulated reflectance is a very strong indication that the woodpile is preserved through the  $\text{SiO}_2$  deposition and polymer removal. The slight blue-shift of the experimentally observed peak at slightly be-

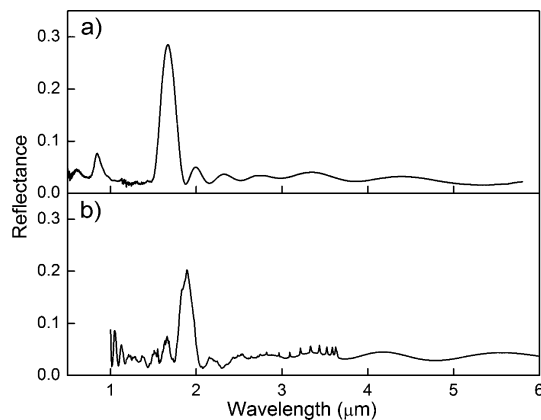


**Figure 4.** Reflectance spectra for  $\text{SiO}_2$  hollow-woodpile (8-layer structure,  $d=2.8 \mu\text{m}$ ): a) experimental and b) simulated.

low 2  $\mu\text{m}$  with respect to the simulated spectrum may indicate a slight contraction of the woodpile during polymer burn-out, or may simply be that we underestimated the amount of  $\text{SiO}_2$  deposited during CVD. The simulation assumes a  $\text{SiO}_2$  wall thickness of 100 nm. If the actual thickness is less, the reflectance peak should blue-shift.

The influence of each processing step on the optical properties of these woodpile-based structures is illustrated in Figure 5. Upon  $\text{SiO}_2$  deposition, the reflectance peaks of the  $\text{SiO}_2$ /polymer woodpile shift to longer wavelengths because the additional material increases its average refractive index.

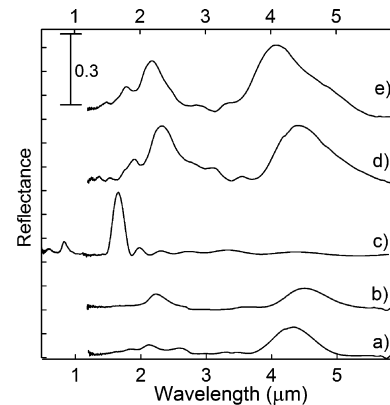


**Figure 5.** Reflectance spectra for a 3D microperiodic structure (8-layer structure,  $d=2.8 \mu\text{m}$ ): a) Polymer woodpile; b)  $\text{SiO}_2$ /polymer woodpile; c)  $\text{SiO}_2$  hollow-woodpile; d)  $\text{Si/SiO}_2/\text{Si}$  hollow-woodpile; and e)  $\text{Si}$  hollow-woodpile after HF etch.

Essentially, a small fraction of the air voids within the structure are replaced with  $\text{SiO}_2$ . The dramatic blue-shift of the optical features upon polymer removal stems from the significant reduction in the average refractive index, as the polymer is now replaced with air. Following Si CVD, a remarkable red-shift is observed in the diffraction peaks due to an increase in its average refractive index. Finally, the  $\text{SiO}_2$  scaffold was removed through HF etching, resulting in a slight blue-shift of the diffraction peaks. Because of the structural complexity of the hollow-woodpile after Si deposition, we have yet to simulate its optical properties; however, the general blue-shift of the optical features fits the expected behavior.

We cannot definitively explain why these Si hollow-woodpiles exhibit a relatively low reflectance ( $\sim 0.3$ ). Prior results reported for woodpile structures comprised of dense Si rods have shown large transmission dips,<sup>[9]</sup> and Si inverse opal structures have large reflectance peaks.<sup>[17,30]</sup> Our woodpiles presently possess a limited number of layers and their topology has not yet been optimized, so it is likely possible to enhance their reflectance by further geometric modifications.<sup>[31,32]</sup> For example, the trilayer  $\text{Si/SiO}_2/\text{Si}$  coating may not provide a sufficient filling fraction of the high-refractive-index material needed for strong optical reflectance. Additionally, inhomogeneities in these structures may further degrade their optical properties. If complete Si infilling is neces-

sary, it should be possible to create dense Si woodpile structures by first filling the entire void space within the polymeric scaffold with SiO<sub>2</sub>, followed by polymer removal, Si CVD, and then etching. A similar procedure has been successfully demonstrated by Ozin et al. in this issue.<sup>[33]</sup>

In summary, Si hollow-woodpile photonic crystals have been fabricated using polyelectrolyte scaffolds as templates. Our procedure is based on a sequential SiO<sub>2</sub>/Si CVD process that results in a 3D microperiodic network of interconnected hollow cylinders, yielding, for the first time, a hollow-woodpile photonic crystal. The optical properties of these 3D microperiodic woodpiles were measured after each processing step, and both the dense polymer and hollow SiO<sub>2</sub> woodpiles were simulated using the transfer-matrix method.<sup>[34]</sup> The maximum observed reflectance of the final Si hollow-woodpile was 0.3. Further experiments and modeling are needed to fully understand their optical response and to guide the writing process to create the desired optical scaffold topography. Direct ink writing may provide a facile route to creating photonic crystals with embedded functionalities on a wide range of substrate materials, and, as demonstrated, opens up a new route for fabricating 3D Si structures of arbitrary design at the microscale. Along with photonic applications, these structures may serve as a novel starting point for many new applications, including Si-based microfluidic networks and low-cost MEMS, where their hollow nature may be ideal for heat-transfer applications and reduced inertial forces.

## Experimental

**3D Polymer Woodpile Fabrication:** 3D microperiodic woodpiles were assembled by depositing a concentrated polyelectrolyte ink ([COONa]/[NH<sub>4</sub>]<sup>+</sup> = 5.7:1) using a computer-aided, direct-write program (IlliniCAD) that controls the three-axis micropositioner stage (ABL 90010 *x*-*y*-*z* motion stage, Aerotech, Inc., Pittsburgh, PA). The ink was dispensed through a pulled borosilicate glass nozzle (1 μm in diameter μ-Tip, World Precision Instruments, Inc., Sarasota, FL) under an applied pressure (800 Ultra dispensing system, EFD Inc.) required to maintain a constant flow rate at a deposition speed of 250 μm s<sup>-1</sup>. 3D face-centered tetragonal lattices were assembled by patterning an array of parallel (rodlike) filaments in the *x*-*y* plane such that their orientation was orthogonal to the previous layer. The face-centered geometry was achieved by shifting alternating *x* and *y* layers by 1/2 the in-plane center-to-center rod spacing. The ambient temperature and humidity were recorded throughout the assembly process, and structures were dried in a desiccator if the ambient humidity was greater than 35 %.

**3D Si Hollow-Woodpile Fabrication:** A thin SiO<sub>2</sub> coating was first deposited onto the polyelectrolyte scaffold surface using chemical vapor deposition under ambient temperature and pressure [16]. Water vapor was flowed over the structure for 90 s to hydrate its surface prior to introducing a stream of SiCl<sub>4</sub>(g)-saturated N<sub>2</sub> that passed over the structure at 6 mL min<sup>-1</sup> for 90 s. The SiCl<sub>4</sub> reacted with water on the woodpile surface to form a thin SiO<sub>2</sub> coating. A small reaction window exists for optimal SiO<sub>2</sub> coverage. A reaction time of 60 s resulted in a SiO<sub>2</sub> layer too thin to withstand further processing steps, while a reaction time of 120 s completely filled the structure, preventing further material deposition. After the SiO<sub>2</sub> layer was deposited, the polymer scaffold was removed by heat treatment. The woodpile was placed in a tube furnace, heated at 1 °C min<sup>-1</sup> to 475 °C, and held for 3 h to burn out the polymer, leaving behind hollow SiO<sub>2</sub> cylinders.

Si was then grown on the surface of the SiO<sub>2</sub> hollow-woodpile via chemical vapor deposition using disilane (Si<sub>2</sub>H<sub>6</sub>) as the precursor gas [32]. The sample was loaded into a reaction vessel where a vacuum was pulled (~10<sup>6</sup> mbar, 1 mbar = 100 Pa) to remove air. Disilane was condensed with liquid N<sub>2</sub> in another chamber and isolated at ~20 mbar. The reaction vessel was then inserted into a vertical-tube furnace set at 375 °C. The decomposition reaction proceeded for 2.5 h, depositing amorphous Si on the inside and outside of the hollow SiO<sub>2</sub> cylinders.

**Spectroscopy:** Reflection spectra were measured with a Fourier-transform infrared spectrometer (Bruker Vertex 70, global lamp) combined with an infrared microscope (Bruker Hyperion 2000 and a liquid-nitrogen-cooled InSb detector). The objective was a 15× Cassegrain with a numerical aperture of 0.4. Light impinged the sample at an angle centered around 16.7° with respect to the sample normal. A square with a 50 μm × 50 μm area was defined by a knife-edge aperture in the light path of the microscope. Spectra were normalized to a silver mirror. The homogeneity tended to decrease near the edge of the samples, so all measurements were acquired within the central regions of the samples. Away from the edges, no significant variations in the optical quality were observed in the samples.

**Simulations:** The calculations were done using the transfer-matrix method in a momentum-space representation. In this approach, the film is discretized along the propagation direction into small segments. The T-matrix (i.e., the transfer matrix, which relates the wave amplitudes from one side of the film to the other side) for each segment is then determined directly from Maxwell's equations. In principle, all these T-matrices could be multiplied to produce the T-matrix of the whole film from which the transmission and reflection coefficients of the film could be determined. However, direct cascading of the T-matrix leads to numerical instability. We overcame the numerical instability by converting the T-matrix to the S-matrix (i.e., the scattering matrix, which relates the outgoing waves to the incoming waves) for each segment, and cascading these S-matrices together [34]. In doing so, for each segment, we expressed the electric and magnetic fields in the incoming waves and outgoing waves in a plane-wave basis with the wave vectors determined by the Bloch theorem, and retained the coefficients for only the lowest reciprocal lattice vectors in the two-dimensional lattice. For each reciprocal lattice vector, we retained the plane waves with both polarizations, as well as the incoming and outgoing waves. This representation thus contains the full polarization and angular information, so that all incidence angles could be treated. Simulations matched the actual spectroscopic conditions and included all azimuthal angles and polarizations. Polymer woodpiles were simulated assuming a rod diameter of 1 μm, polymer *n* = 1.5, layer-to-layer spacing in the *z*-direction of 950 nm (5 % overlap between layers), and substrate *n* = 1.5. The hollow SiO<sub>2</sub> coating was taken to be 100 nm thick, SiO<sub>2</sub> *n* = 1.42, and substrate *n* = 1.5.

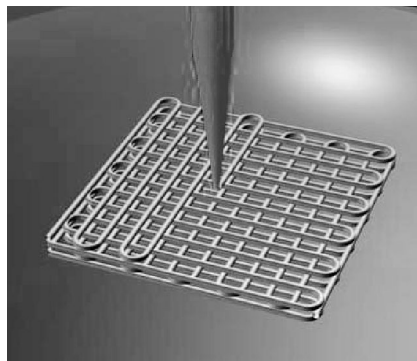
Received: July 15, 2005

Final version: December 20, 2005

- [1] H. S. Rong, R. Jones, A. S. Liu, O. Cohen, D. Hak, A. Fang, M. Paniccia, *Nature* **2005**, 433, 725.
- [2] *Silicon Photonics* (Eds: L. Pavesi, D. J. Lockwood), Springer, Berlin **2004**.
- [3] G. T. Reed, A. P. Knights, *Silicon Photonics: An Introduction*, Wiley, Chichester, UK **2004**.
- [4] S. M. Weiss, M. Haurylau, P. M. Fauchet, *Opt. Mater.* **2005**, 27, 740.
- [5] J. W. Judy, *Smart Mater. Struct.* **2001**, 10, 1115.
- [6] H. Andersson, A. van den Berg, *Lab Chip* **2004**, 4, 98.
- [7] G. H. W. Sanders, A. Manz, *TrAC, Trends Anal. Chem.* **2000**, 19, 364.
- [8] T. Ito, S. Okazaki, *Nature* **2000**, 406, 1027.
- [9] S. Y. Lin, J. G. Fleming, D. L. Hetherington, B. K. Smith, R. Biswas, K. M. Ho, M. M. Sigalas, W. Zubrzycki, S. R. Kurtz, J. Bur, *Nature* **1998**, 394, 251.
- [10] S. Noda, K. Tomoda, N. Yamamoto, A. Chutinan, *Science* **2000**, 289, 604.

- [11] J. A. Lewis, G. M. Gratson, *Mater. Today* **2004**, 7(7–8), 32.
- [12] B. H. Cumpston, S. P. Ananthavel, S. Barlow, D. L. Dyer, J. E. Ehrlich, L. L. Erskine, A. A. Heikal, S. M. Kuebler, I. Y. S. Lee, D. McCord-Maughon, J. Q. Qin, H. Rockel, M. Rumi, X. L. Wu, S. R. Marder, J. W. Perry, *Nature* **1999**, 398, 51.
- [13] M. Deubel, G. von Freymann, M. Wegener, S. Pereira, K. Busch, C. Soukoulis, *Nat. Mater.* **2004**, 3, 444.
- [14] G. M. Gratson, M. Xu, J. A. Lewis, *Nature* **2004**, 428, 386.
- [15] G. M. Gratson, J. A. Lewis, *Langmuir* **2005**, 21, 457.
- [16] H. Miguez, N. Tetreault, B. Hatton, S. M. Yang, D. Perovic, G. A. Ozin, *Chem. Commun.* **2002**, 2736.
- [17] A. Blanco, E. Chomski, S. Grabtchak, M. Ibisate, S. John, S. W. Leonard, C. Lopez, F. Meseguer, H. Miguez, J. P. Mondia, G. A. Ozin, O. Toader, H. M. von Driel, *Nature* **2000**, 405, 437.
- [18] J. D. Joannopoulos, P. R. Villeneuve, S. Fan, *Nature* **1997**, 386, 143.
- [19] T. Yamamoto, J. Yamaguchi, N. Takeuchi, A. Shimizu, R. Sawada, E. Higurashi, Y. Uenishi, *Jpn. J. Appl. Phys., Part 1* **2004**, 43, 5824.
- [20] J.-M. Koo, S. Im, L. Jiang, K. E. Goodson, *J. Heat Transfer* **2005**, 127, 49.
- [21] A. Ressine, S. Ekstrom, G. Marko-Varga, T. Laurell, *Anal. Chem.* **2003**, 75, 6968.
- [22] E. Yablonovitch, *Phys. Rev. Lett.* **1987**, 58, 2059.
- [23] S. John, *Phys. Rev. Lett.* **1987**, 58, 2486.
- [24] K. M. Ho, C. Soukoulis, K. Constant, M. M. Sigalas, Z. Z. Chen, R. Biswas, J. D. Joannopoulos, *Solid State Commun.* **1994**, 89, 413.
- [25] H. S. Sozuer, J. P. Dowling, *J. Mod. Opt.* **1994**, 41, 231.
- [26] A. Chutinan, S. Noda, *Appl. Phys. Lett.* **1999**, 75, 3739.
- [27] W. Lee, S. A. Pruzinsky, P. V. Braun, *Adv. Mater.* **2002**, 14, 271.
- [28] A. B. Zezin, V. A. Kabanov, *Russ. Chem. Rev.* **1982**, 51, 833.
- [29] A. Zintchenko, R. Rother, H. Dautzenberg, *Langmuir* **2003**, 19, 2507.
- [30] Y. A. Vlasov, X. Z. Bo, J. C. Sturm, D. J. Norris, *Nature* **2001**, 414, 289.
- [31] K. Busch, S. John, *Phys. Rev. E: Stat. Phys., Plasmas, Fluids, Relat. Interdiscip. Top.* **1998**, 58, 3896.
- [32] F. García-Santamaría, M. Ibisate, I. Rodriguez, F. Meseguer, C. Lopez, *Adv. Mater.* **2003**, 15, 788.
- [33] N. Tetreault, G. von Freymann, M. Deubel, M. Hermatschweiler, F. Pérez-Willard, S. John, M. Wegener, G. A. Ozin, *Adv. Mater.*, 11 October 2005, DOI: 10.1002/adma.200501674.
- [34] J. B. Pendry, A. MacKinnon, *Phys. Rev. Lett.* **1992**, 69, 2772.

**3D Si hollow-woodpile photonic crystals** are formed through the direct-write assembly of concentrated polyelectrolyte inks (rods ~1 μm in diameter) followed by a sequential silica/silicon chemical vapor deposition process (see Figure). The direct conversion of 3D polymer microstructures to materials like silicon may enable such applications as photonic materials, low-cost microelectromechanical systems (MEMS), microfluidic networks for heat dissipation, and biological devices.



## COMMUNICATIONS

### Photonic Crystals

G. M. Gratson, F. García-Santamaría, V. Lousse, M. Xu, S. Fan, J. A. Lewis,\* P. V. Braun\* ..... ■ – ■

**Direct-Write Assembly of Three-Dimensional Photonic Crystals: Conversion of Polymer Scaffolds to Silicon Hollow-Woodpile Structures**